Fully automatic *p*-adaptive hybrid-Trefftz displacement elements

A.H. Jesus[1]* **and I. Cismaşiu**[1] **and J.A.T. Freitas**[2]

[1] *UNIC, Departamento de Engenharia Civil, Faculdade de Ciências e Tecnologia, FCT, Universidade Nova de Lisboa, Quinta da Torre, 2829-516 Monte de Caparica, Portugal*
e-mail: andrehjesus@gmail.com / ildi@fct.unl.pt

[2] *Departamento de Engenharia Civil e Arquitectura, Instituto Superior Técnico Av. Rovisco Pais, 1096-001 Lisboa, Portugal*
e-mail: freitas@civil.ist.utl.pt

Abstract

This paper reports on the implementation details of a fully automatic *p*-adaptive procedure to select the approximation bases of the displacement model of the hybrid-Trefftz finite element formulation. The formulation allows for the direct approximation and enrichment of two independent fields, the displacements in the domain and the surface forces on the element boundaries. By controlling the strain energy of the system for a prescribed finite element mesh, the *p*-adaptive algorithm uses the nonconformity and nonequilibrium error minimization criteria to identify the boundary and domain regions where the degree of the surface force and displacement bases should be increased or alternatively in which elements the kinematic indeterminacy number of the domain bases should be enriched. Numerical results demonstrate the efficiency of the algorithm and the feasibility of carrying out automatic *p*-adaptive enrichment in 2D elastostastic analyses.

Keywords: Hybrid-Trefftz displacement model, p-adaptivity, 2D elasticity

1. Introduction

The hybrid-Trefftz displacement formulation requires the simultaneous approximation of two fields, the displacements in the domain and the surface forces on the element boundary.

The domain approximation basis must satisfy simultaneously the equilibrium, compatibility and constitutive conditions or their combination in the Navier description of the governing differential equation.

The inter-element continuity and the kinematic boundary conditions are enforced on average using the independent surface force approximation basis.

The implementation approach consists in accepting both the domain and the boundary finite element degrees of freedom as explicit variables. The finite element mesh is built on few elements with a general geometry. They may not be bounded, convex or simply connected and they may have an arbitrary number of sides with parametric description as the approximation functions are not associated to nodes.

The *p*-adaptive procedure presented in this paper is designed to allow the automatic selection of the optimal order of the approximation functions on the domain of the element and on its boundaries to obtain a given level of accuracy.

This accuracy is measured on the strain energy of the system for a prescribed finite element mesh.

The present work extends into elastostatic analysis [4] the *p*-adaptive procedure originally reported for Laplace problems [5].

2. Finite element framework

The finite element model being used develops from the independent approximation of the displacement and traction fields in each domain V^e and on the Dirichlet boundary, Γ_u^e.

The displacement field in the domain V^e is approximated as a linear combination of the displacement approximation functions:

$$\boldsymbol{u} = \boldsymbol{U}_1 \boldsymbol{q}_1 + \boldsymbol{U}_2 \boldsymbol{q}_2 + \boldsymbol{u}_p \ \text{ in } V^e \tag{1}$$

Matrices $\boldsymbol{U}_1$ and $\boldsymbol{U}_2$ collect the strain inducing functions selected from the solution of the governing differential equation of the problem and the rigid body modes, respectively. Vectors $\boldsymbol{q}_1$ and $\boldsymbol{q}_2$ contains the weights of the linear combination, representing generalized displacements. Vector $\boldsymbol{u}_p$ can be used to include particular solutions.

The surface forces are independently approximated on every inter-element boundary and for every boundary of the assembled structure whereon the displacements are prescribed, Γ_u^e:

$$\boldsymbol{t} = \boldsymbol{T}\boldsymbol{p} \ \text{ on } \Gamma_u \tag{2}$$

Matrix $\boldsymbol{T}$ collects surface forces approximation functions and the weighing vector $\boldsymbol{p}$ represent generalized surfaces forces.

By imposing the compatibility on all sides that do not belong to the static boundaries and equilibrium in all elements in a weighted residual form, following the procedure described in [4], the finite element governing system is:

$$\begin{bmatrix} \boldsymbol{K} & \boldsymbol{O} & -\boldsymbol{B}_1 \\ \boldsymbol{O} & \boldsymbol{O} & -\boldsymbol{B}_2 \\ -\boldsymbol{B}_1^T & -\boldsymbol{B}_2^T & \boldsymbol{O} \end{bmatrix} \begin{Bmatrix} \boldsymbol{q}_1 \\ \boldsymbol{q}_2 \\ \boldsymbol{p} \end{Bmatrix} = \begin{Bmatrix} \boldsymbol{X}_{01} \\ \boldsymbol{X}_{02} \\ -\boldsymbol{v}_\Gamma \end{Bmatrix} \tag{3}$$

The finite element arrays present in system (3) are defined by boundary integral expressions, as follows:

$$\boldsymbol{K} = \int \boldsymbol{U}_1^T \boldsymbol{T}_1 \, \mathrm{d}\Gamma^e \tag{4}$$

$$\boldsymbol{B}_i = \int \boldsymbol{U}_i^T \boldsymbol{T} \, \mathrm{d}\Gamma_u^e \quad i = 1, 2 \tag{5}$$

* Research grant founded by project PTDC/ECM/70781/2006

$$\boldsymbol{X}_{0i} = \int \boldsymbol{U}_i^T \boldsymbol{t}_\Gamma \, \mathrm{d}\Gamma_\sigma^e \quad i=1,2 \tag{6}$$

$$\boldsymbol{v}_\Gamma = \int \boldsymbol{T}^T \boldsymbol{u}_\Gamma \, \mathrm{d}\Gamma_u^e \tag{7}$$

The structure of the governing system for the assembled mesh is identical to that of the elementary system, featuring a highly sparse format and a quasi-uncoupled form, as the generalised displacements $\boldsymbol{q}_1$ and $\boldsymbol{q}_2$ are strictly element dependent and the generalised surface forces $\boldsymbol{p}$ are shared at most by two connecting domain elements. Matrix $\boldsymbol{K}$ is block diagonal and collects the elementary stiffness matrices (4). The boundary equilibrium matrices $\boldsymbol{B}_i$ are associated with the surface force vector shared by domain elements connecting on the same boundary element $\Gamma_{u_i}^e$.

This structure is particularly well suited to adaptive *p*-refinement [5] and parallel processing [2].

3. Design of the mesh

To perform analyses with hybrid-Trefftz displacement elements the number of options the analyst faces in designing the mesh is wide, as each element may have a different number of sides and different approximation bases (1) and (2) can be implemented in the domain and on the boundary of the element.

This decision has a direct effect on the quality and, eventually, on the stability of the solution, and cannot be handled safely and efficiently by inexperienced users.

The elementary approximation bases (1) are non-nodal and naturally hierarchical, selected from the solution of the governing differential equation of the problem.

No constraints are placed a priori on the surface approximation functions (2), namely in what concerns regularity and continuity. However, to ensure convergence, the surface forces approximation basis $\boldsymbol{T}$ is assumed to be contained in traction basis induced by the domain approximation.

In particular, the relative dimensions of the domain and boundary approximation bases cannot be set independently.

For example, in two-dimensional elastostatic applications with $\boldsymbol{u}_p = 0$, matrix $\boldsymbol{U}_2$ and $\boldsymbol{U}_1$ collect three rigid-body modes and $3+4(d_u-1)$ strain-inducing polynomial modes, respectively, yielding n_u^e degrees of freedom:

$$n_u^e = 2 + 4\,d_u \tag{8}$$

The dimension of the polynomial terms of degree in the traction mode matrix $\boldsymbol{T}$ in approximation (2) is,

$$n_t^e = \sum_{i=1}^{n_b} \alpha_n^i (d_{tn}+1) + \alpha_t^i (d_{tt}+1) \tag{9}$$

where $d_{t(n/t)}$ is the degree of traction approximations on normal and tangential direction and $\alpha_{n/t}^i = 1$ if traction components are approximated on n or t direction.

Under the assumption that the elementary approximation bases (1) and (2) are complete and linearly independent, the domain degrees of freedom are necessarily independent and the following condition on the kinematic indeterminacy number of the element,

$$\beta_e = n_u^e - n_t^e \geq 0 \tag{10}$$

is, in general, sufficient to ensure that the same property holds for the boundary degrees of freedom of the assembled mesh, to yield:

$$\beta_{str} = N_q - N_p \geq 3 \tag{11}$$

However, due to the vectorial nature of the conformity condition (3.c), the conditions above may not be sufficient to ensure that a particular continuity condition is not over constrained (10), which may lead to the development of spurious modes in the solution.

The sources of error that affect this type of element are the lack of conformity either between connecting elements or on the Dirichlet boundary and the lack of equilibrium between the assumed tractions (2) and the tractions induced by the displacement approximation (1).

4. Selective *p*-adaptive procedure

The *p*-adaptive algorithm presented here uses the nonconformity and non-equilibrium error minimization criterion to identify the boundary and domain regions where the degree of the surface force and displacement bases should be increased.

4.1. Enrichment of the domain approximation basis

Assume that a new strain-inducing displacement mode $\bar{U}_1$ is added to the approximation (1) in a particular domain element, with $\boldsymbol{u}_p = 0$.

The enriched displacement approximation,

$$\boldsymbol{u} = \boldsymbol{U}_1(\boldsymbol{q}_1 + \Delta\boldsymbol{q}_1) + \boldsymbol{U}_2(\boldsymbol{q}_2 + \Delta\boldsymbol{q}_2) + \bar{U}_1 \Delta\bar{q}_1 \tag{12}$$

adds a new degree of freedom to the solution $\Delta\bar{q}_1$ and produces a variation,

$$\Delta\boldsymbol{x}^T = [\Delta\boldsymbol{q}_1 \;\; \Delta\boldsymbol{q}_2 \;\; \Delta\boldsymbol{p}] \tag{13}$$

on the current solution $\boldsymbol{x}^T = [\boldsymbol{q}_1 \;\; \boldsymbol{q}_2 \;\; \boldsymbol{p}]$. A new equilibrium equation is added to the solving system (3), which extends to:

$$\begin{bmatrix} \boldsymbol{K} & \bar{\boldsymbol{K}}_1 & \boldsymbol{O} & -\boldsymbol{B}_1 \\ \bar{\boldsymbol{K}}_1^T & \bar{K} & \boldsymbol{O} & -\bar{\boldsymbol{B}}_1 \\ \boldsymbol{O} & \boldsymbol{O} & \boldsymbol{O} & -\boldsymbol{B}_2 \\ -\boldsymbol{B}_1^T & -\bar{\boldsymbol{B}}_1^T & -\boldsymbol{B}_2^T & \boldsymbol{O} \end{bmatrix} \begin{Bmatrix} \boldsymbol{q}_1 + \Delta\boldsymbol{q}_1 \\ \Delta\bar{q}_1 \\ \boldsymbol{q}_2 + \Delta\boldsymbol{q}_2 \\ \boldsymbol{p} + \Delta\boldsymbol{p} \end{Bmatrix} = \begin{Bmatrix} \boldsymbol{X}_{01} \\ \Delta\bar{X}_{01} \\ \boldsymbol{X}_{02} \\ -\boldsymbol{v}_\Gamma \end{Bmatrix} \tag{14}$$

The contribution of the new degree of freedom to the stiffness matrix, $\bar{\boldsymbol{K}}_1$ and $\bar{K}$, is computed from definition (4) and the equilibrium matrix $\bar{\boldsymbol{B}}_1$ from (5). The non-null entries of vector $\bar{\boldsymbol{K}}_1$ are associated with the domain degrees of freedom $\boldsymbol{q}_1$ assigned to the enriched domain element. All entries of vector $\bar{\boldsymbol{B}}_1$ are null except for those that are associated with the degrees of freedom of variable $\boldsymbol{p}$ assigned to the boundary of the enriched domain element. Scalar $\Delta\bar{X}_{01}$ is computed using definition (6) for the a boundary of the enriched element whereon a non-homogeneous Neumann condition holds.

The compact form of the extended solving system is:

$$\begin{bmatrix} \boldsymbol{A} & \bar{\boldsymbol{C}} \\ \bar{\boldsymbol{C}}^T & \bar{K} \end{bmatrix} \begin{Bmatrix} \Delta\boldsymbol{x} \\ \Delta\bar{q}_1 \end{Bmatrix} = \begin{Bmatrix} \boldsymbol{O} \\ \Delta\bar{X}_{01} - \bar{X}_{01} \end{Bmatrix} \tag{15}$$

where

$$\bar{\boldsymbol{C}}^T = [\bar{\boldsymbol{K}}_1^T \;\; \boldsymbol{O} \;\; -\bar{\boldsymbol{B}}_1] \tag{16}$$

$$\bar{X}_{01} = \bar{\boldsymbol{K}}_1^T \boldsymbol{q}_1 - \bar{\boldsymbol{B}}_1^T \boldsymbol{p} \tag{17}$$

The variation on the current solution $\Delta\boldsymbol{x} = \dot{\boldsymbol{x}}\Delta\bar{q}_1$ is obtained after computing the gradient $\dot{\boldsymbol{x}}$ of the current solution, from Eqn. (15.a), using the factorized form of the previous system matrix $\boldsymbol{A}$, and the new degree of freedom $\Delta\bar{\boldsymbol{q}}_1$ from (15.b):

$$\Delta\bar{q}_1 = (\Delta\bar{X}_{01} - \bar{X}_{01}) / \dot{X_{01}} \tag{18}$$

with $\dot{X}_{01} = \bar{K} + \bar{\boldsymbol{C}}^T \dot{\boldsymbol{x}}$. The variation in the strain energy ΔU is determined from the incremental form of the following definition:

$$\Delta U = (\dot{U} + \bar{\boldsymbol{K}}_1^T \boldsymbol{q}_1)\Delta\bar{q}_1 + \frac{1}{2}(\ddot{U} + 2\bar{\boldsymbol{K}}_1^T \dot{\boldsymbol{q}}_1 + \bar{K})(\Delta\bar{q}_1)^2 \tag{19}$$

with $\dot{U} = \dot{\boldsymbol{q}}_1^T \boldsymbol{K} \boldsymbol{q}_1$ and $\ddot{U} = \dot{\boldsymbol{q}}_1^T \boldsymbol{K} \dot{\boldsymbol{q}}_1$

A spurious mode is added to the displacement approximation basis when $\dot{X}_{01} = 0$ in (18) and consequently has no solution when this result combines with $\Delta\bar{X}_{01} - \bar{X}_{01} \neq 0$ and is undetermined otherwise.

The error in equilibrium added to the domain approximation is defined as,

$$\varepsilon_V = (\Delta\bar{X}_{01} - \bar{X}_{01})/V \tag{20}$$

and V represents the surface of the domain element.

4.2. Enrichment of the boundary approximation basis

Assume that the surface forces approximation (2) in a particular boundary element is enriched by adding a new degree of freedom $\Delta\bar{p}$, to produce a variation $\Delta\boldsymbol{p}$ of the current solution $\boldsymbol{p}$.

The traction approximation enriched with $\bar{T}$,

$$\boldsymbol{t} = \boldsymbol{T}(\boldsymbol{p} + \boldsymbol{\Delta p}) + \bar{T}\Delta\bar{p} \tag{21}$$

leads to a new compatibility equation to the solving system (3), which extends to:

$$\begin{bmatrix} \boldsymbol{K} & \boldsymbol{O} & -\boldsymbol{B}_1 & -\bar{\boldsymbol{B}}_1 \\ \boldsymbol{O} & \boldsymbol{O} & -\boldsymbol{B}_2 & -\bar{\boldsymbol{B}}_2 \\ -\boldsymbol{B}_1^T & -\boldsymbol{B}_2^T & \boldsymbol{O} & \boldsymbol{O} \\ -\bar{\boldsymbol{B}}_1^T & -\bar{\boldsymbol{B}}_2^T & \boldsymbol{O} & \boldsymbol{O} \end{bmatrix} \begin{Bmatrix} \boldsymbol{q}_1 + \Delta\boldsymbol{q}_1 \\ \boldsymbol{q}_2 + \Delta\boldsymbol{q}_2 \\ \boldsymbol{p} + \Delta\boldsymbol{p} \\ \Delta\bar{p} \end{Bmatrix} = \begin{Bmatrix} \boldsymbol{X}_{01} \\ \boldsymbol{X}_{02} \\ -\boldsymbol{v}_\Gamma \\ -\Delta\bar{v}_\Gamma \end{Bmatrix} \tag{22}$$

or in compact form:

$$\begin{bmatrix} \boldsymbol{A} & -\bar{\boldsymbol{B}} \\ -\bar{\boldsymbol{B}}^T & \boldsymbol{O} \end{bmatrix} \begin{Bmatrix} \Delta\boldsymbol{x} \\ \Delta\bar{p} \end{Bmatrix} = \begin{Bmatrix} \boldsymbol{O} \\ \bar{v}_\Gamma - \Delta\bar{v}_\Gamma \end{Bmatrix} \tag{23}$$

where the following definitions are adopted,

$$\bar{\boldsymbol{B}}^T = [\bar{\boldsymbol{B}}_1^T \; \bar{\boldsymbol{B}}_2^T \; \boldsymbol{O}] \tag{24}$$

$$\bar{v}_\Gamma = \bar{\boldsymbol{B}}_1^T \boldsymbol{q}_1 + \bar{\boldsymbol{B}}_2^T \boldsymbol{q}_2 \tag{25}$$

Vectors $\bar{\boldsymbol{B}}_i \, (i = 1, 2)$ and scalar $\Delta\bar{v}_\Gamma$ are computed from definition (5) and (7) for the newly added polynomial function $\bar{T}$.

The variation on the current solution

$$\Delta\boldsymbol{x} = \dot{\boldsymbol{x}}\Delta\bar{p} \tag{26}$$

is obtained after computing the gradient $\dot{\boldsymbol{x}}$ of the current solution with respect to the added degree of freedom, from (23.a), using the factorized form of the previous system matrix, and $\Delta\bar{\boldsymbol{p}}$ computed from (23.b):

$$\Delta\bar{p} = (\Delta\bar{v}_\Gamma - \bar{v}_\Gamma)/\dot{v}_\Gamma \tag{27}$$

$$\dot{v}_\Gamma = \bar{\boldsymbol{B}}_1^T \dot{\boldsymbol{q}}_1 + \bar{\boldsymbol{B}}_2^T \dot{\boldsymbol{q}}_2 \tag{28}$$

The increment on the strain energy of the system is computed from the following definition:

$$\Delta U = (\dot{\boldsymbol{q}}_1^T \boldsymbol{K} \boldsymbol{q}_1)\Delta\bar{\boldsymbol{p}} + \frac{1}{2}(\dot{\boldsymbol{q}}_1^T \boldsymbol{K} \dot{\boldsymbol{q}}_1)\Delta\bar{\boldsymbol{p}}^2 \tag{29}$$

A spurious q-mode is exposed when $\dot{v}_\Gamma = 0$ in (28) and consequently has no solution when this result combines with $\Delta\bar{v}_\Gamma - \bar{v}_\Gamma \neq 0$.

The error density in conformity on the boundary element of length L for the degree of freedom added to the boundary approximation bases is defined as,

$$\varepsilon_\Gamma = (\Delta\bar{v}_\Gamma - \bar{v}_\Gamma)/L \tag{30}$$

5. Refinement strategy

The objective of a *p*-refinement algorithm is to find the optimal sequence of combinations for the degrees of freedom of the approximation in each domain and boundary element that ensures the convergence of the finite element solution.

The optimal criterion of the *p*-adaptive process for problems modelled by conforming elements is the minimization (maximization) of the strain energy for the assembled mesh. However, the *p*-refinement of the solutions produced by the hybrid displacement models do not, in general, induce a monotone convergence on strain energy as the hybrid displacement elements do not, in general, produce kinematically admissible solutions [1, 3].

The *p*-adaptive algorithm was developed with two independent domain enrichment criteria in combination with the boundary approximation basis enrichment strategy described in Section 4.2.

The first approach uses the kinematic indeterminacy number to ensure hyperkinematic solutions at both element ($\beta_e > 0$) and structure ($\beta_{str} \geq 3$) levels.

The second approach uses the minimization of the sources of error of the hybrid-Trefftz displacement model, namely the error in equilibrium and in conformity for the degrees of freedom added to the domain and boundary approximation bases, (20) and (30).

5.1. Fast p*-adaptive algorithm*

The algorithm described below combines the enrichment of the boundary basis directed by the largest conformity error density (30) and the enrichment of the domain basis to ensure hyper kinematic solutions. The progressive constraining of the solution is implemented by adding one boundary degree of freedom at each step. To ensure that the domain basis is complete, an even number of degrees of freedom is added whenever this operation of global relaxation is implemented.

The implementation of the boundary basis enrichment has a reduced computational complexity compared with the alternative of enriching the domain basis. This algorithm is termed *fast* and its pseudo code develops as follows:

Input: initial uniform approximation (d_u^0, d_t^0)
Check for $\beta_e > 0$ and $\beta_{str} \geq 3$ and increase d_u if necessary
For each boundary element and each new dof compute: $\dot{v}_\Gamma$ and ε_Γ.
  If spurious modes or indeterminacy condition holds in (28)
    goto (qSPM)
  Endif
  Implement (27), update boundary basis for the largest ε_Γ (30)
  Update β_{str}, check (11) and increase d_u by two if necessary.
  For each element connected to the enriched boundary,
  check for $\beta_e < 0$ and implement:
    (qSPM) Increase d_u by two, update β_e and β_{str}.
    Compute the new solution and update strain energy (29).
  Endfor
  If the $\Delta U < \varepsilon_U$ or highest degree of the approximation bases exceeds the given upper bound.
  Stop
Endfor

5.2. Complete p*-adaptive algorithm*

The second algorithm implements the control of the equilibrium error density (20) minimization criterion to identify the domain elements where the approximation basis should be increased. The enrichment of the boundary basis is directed by the largest conformity error density (30). This algorithm, termed *complete*, obtains a smoother solution, as compared with the fast algorithm, at the expense of increased computational cost and programming complexity. This algorithm, based

on the experience gained, can efficiently and safely identify the optimal dimension of the approximation basis keeping the number of degrees of freedom reduced and providing an efficient preprocessing tool.

The complete *p*-adaptive algorithm develops as follows:
Input: initial uniform approximation (d_u^0, d_t^0) and check d_u^0 for even number
For each domain element and each new dof compute: ε_V (20), $\Delta\bar{q}_1$ (18) and estimate strain energy ΔU (19)
Endfor
For each boundary element and each new dof compute: $\dot{v}_\Gamma$ and ε_Γ (30).
If spurious condition holds for (28)
(qSPM) Increase d_u by two in each element connected to the enriched boundary
Implement (27) estimate strain energy (29)
Endfor
If the $\Delta U/U < \varepsilon_U$ or $d_u, d_t > d_u^m, d_t^m$ **Stop**
For the $\max(\varepsilon_{V_i}, \varepsilon_{\Gamma_i})$ increase d_{u_i} by two or d_{t_i} by one
Compute the new solution and update strain energy using (19) or (29).
Endfor

6. Numerical results

The performance of the *p*-adaptive approach is evaluated using four elastostatic problems.

A polynomial approximation is used for the displacements in the domain elements, selected from the solution of the bi-harmonic stress potential equation governing 2D elastostatic problems for homogeneous and isotropic material.

No particular solutions $\boldsymbol{u}_p$ will be applied during p-refinement tests as is assumed that the decision on the functions to be added and the number and location of the local solution are defined by user. The role of the *p*-adaptive procedure is to select the optimal degrees of the polynomial approximations in each domain d_u^e and on each boundary element, d_t^i.

For problems with "known" strain energy the convergence of the solution is measured using the finite element strain energy U, the energy error norm $|U/U_0|$, and the relative error norm $\varepsilon_U = \sqrt{|1-U/U_0|}$ against the "exact" energy, U_0. Otherwise the converge measure is the variation of energy increase ΔU relative to the current energy $\varepsilon = |\Delta U/U|$.

The initial approximations are uniform and the lowest possible, usually $d_u^0 = 1$ for the displacement approximation in all elements and $d_t = d_{tn}^0 = d_{tt}^0 = 0$ on all sides for traction approximations.

The typical pattern of the enrichment is based on a progressive constraining of the solution, adding a degree d_t sequentially on the boundary (the best strategy in terms of illustration), and eventually a relaxation on the conditions by adding two degrees on the domain d_u.

In all graphs concerning the *p*-adaptive algorithm, the continuous lines represent sequences obtained by increasing the degree on the boundary while keeping constant the degree in the domain. The discontinuities are due to the increase of the degree in the domain for the same degree on the boundary approximation.

6.1. Square plate

The square plate shown in Figure 1, with unit Young's modulus $E = 1$ and Poisson's ratio $\nu = 0.25$, suggested by Robinson [7], is used to test the ability of the *p*-adaptive algorithm to converge to the exact solution.

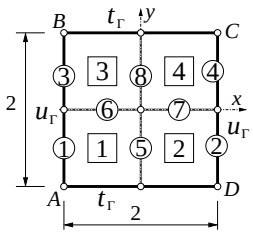

Figure 1: Robinson plate, boundary conditions and FEM discretization.

The problem is solved for the mixed, Dirichlet and Neumann, boundary conditions (on $x = \pm 1$ and $y = \pm 1$) associated with the following analytical solution:

$$u_x = -xy(0.8x^2 + 1.2y^2) \tag{31a}$$

$$u_y = -x^2(x^2 - 3y^2) \tag{31b}$$

$$\sigma_{xx} = -0.32y(3x^2 + 4y^2) \tag{31c}$$

$$\sigma_{yy} = 0.32y(18x^2 - y^2) \tag{31d}$$

$$\sigma_{xy} = -0.96x(2x^2 - y^2) \tag{31e}$$

The convergence pattern of the norm of the relative error in the strain energy normalized by the "exact" value $U = 7.3728$, obtained with a four element mesh, is presented in Figure 2.

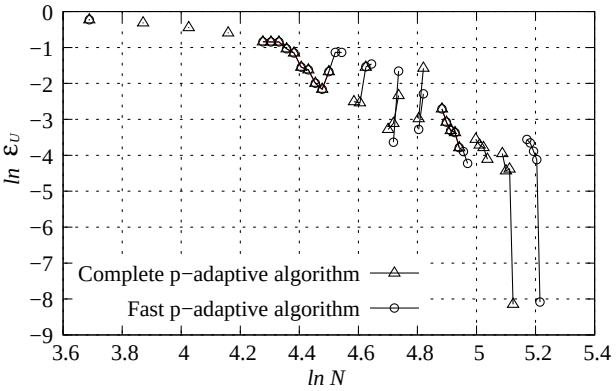

Figure 2: Convergence of the relative error norm in the strain energy (Robinson plate).

The two algorithms show similar convergence patterns for a relative energy error $|\Delta U|/U_0 < 0.001\%$. The initial and final degrees for both algorithms are displayed in Table 1.

Table 1: Approximation degrees and system dimensions for the complete (C) and fast (F) *p*-adaptive algorithms (Robinson plate).

	Domain(d_u)				d_t on all sides	
Step	1	2	3	4	1-8	Dof
1	1	1	1	1	0	40
31(F)	7	7	7	7	3	184
35(C)	5	7	7	5	3	168

The degrees of the approximation of the domain basis in some elements are higher than the minimum required. This is due to the enrichment strategy adopted, described in Section 5, whenever the operation of global relaxation is implemented (10), (11) or when the spurious mode condition (28) verifies, the domain basis, d_u, is increased by two. Possible errors induced by the numerical approximations can also lead to overestimation of the approximations order.

In Figure 3 the numerical results obtained for the σ_{xy} stress field on CB and BA boundaries are compared to the exact solution. Starting from the weakest possible solution the algorithm reaches an accurate solution automatically.

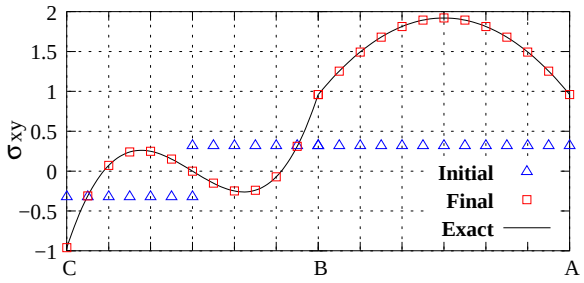

Figure 3: σ_{xy} stress estimates obtained with the complete algorithm on the CB and BA boundaries(Robinson plate).

The displacement and stress fields obtained with complete *p*-adaptive algorithm are shown in Figure 4.

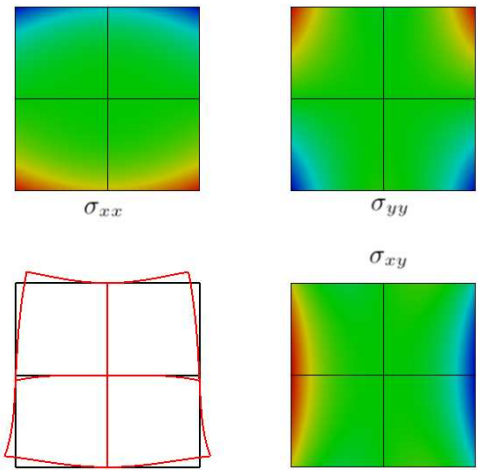

Figure 4: Displacement $[0.06u]$ and stress fields $\sigma_{xx}[-2.2:2.2]$; $\sigma_{yy}[-5.4:5.4]$; $\sigma_{xy}[-1.9:1.9]$ (Robinson plate).

6.2. *Plate with a central crack*

The plate with a central crack subject to uniform tension is used to illustrate the modelling of high stress gradients at the crack tip. The stress intensity factors are extracted from the solution after the conclusion of the *p*-refinement, when the domain approximation is enriched with two independent (Mitchell) crack functions. The weights associated with these functions in the displacement approximation represent the stress intensity factors for modes I and II, which are the opening and shear mode respectively.

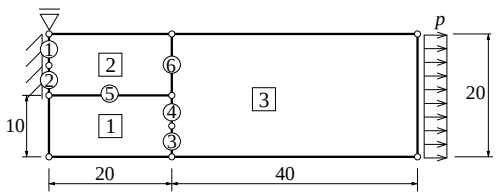

Figure 5: FEM mesh (plate with central crack).

Due to the symmetry only half of the problem is modelled discretized with a three element mesh.

The plate geometry, with measures in mm, the boundary conditions $p = 10$ and the adopted mesh are shown in Figure 5. A unit Young's modulus $E = 1$ and Poisson's ratio $\nu = 0.3$ is used.

Both, the fast and complete, *p*-adaptive algorithms follow the same convergence pattern and need 31 steps to reach convergence for $\varepsilon < 0.001\%$. The strain energy at the end of the enrichment process and before the inclusion of the singular functions, is $U = 85471.5$ obtained for the degrees of approximations presented in Table 2.

Table 2: Degrees in the domain and boundary (plate with a central crack).

	Domain (d_u)			Boundary (d_t)						
Step	1	2	3	1	2	3	4	5	6	Dof
1	1	1	1	0	0	0	0	0	0	29
31	9	9	7	2	3	2	1	7	5	152

The convergence of the strain energy U and the strain energy variation ΔU relatively to the strain energy U is shown in Figure 6 and Figure 7, respectively.

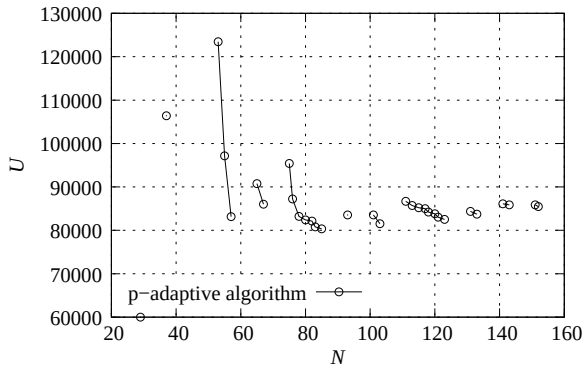

Figure 6: Convergence of the strain energy (plate with a central crack).

The final energy after the enrichment of the domain basis with the singular crack functions is $U = 90502.44$. Similar result $U = 90494.87$ is reported in [1] obtained with uniform degrees yielding a system of 267 degrees of freedom.

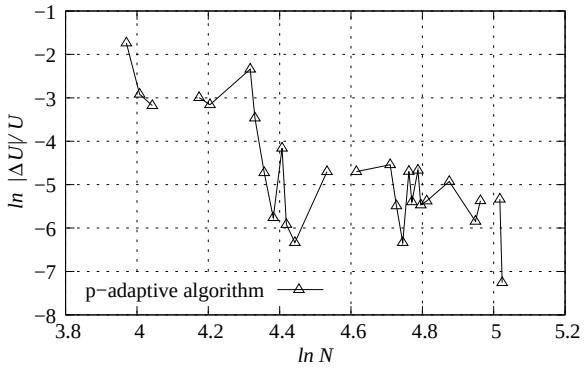

Figure 7: Convergence of the variation of the strain energy (plate with a central crack).

The estimates for the stress intensity factors are $K_I = 160.55$ and $K_{II} = -2.24$, while for an infinite plate the theoretical values

are $K_I = 159.32$ and $K_{II} = 0$ [6]. The finite element solutions for the stress and displacement fields are presented in Figure 8.

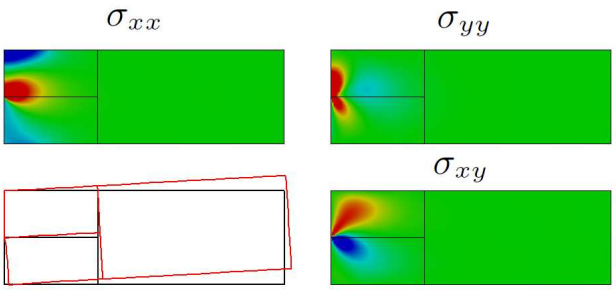

Figure 8: Displacement ($0.001u$) and stress fields $\sigma_{xx}[-7:27]$; $\sigma_{yy}[-9:9]$; $\sigma_{xy}[-9:9]$ (plate with a central crack).

6.3. *Plate with a square hole*

A square plate with a square hole under uniaxial traction with a singularity at wedge point C is considered with $E = 1.0E5$ and $\nu = 0.3$. One quarter of the problem is modelled with a three element regular mesh and four boundaries whereon tractions are prescribed, Figure 9.

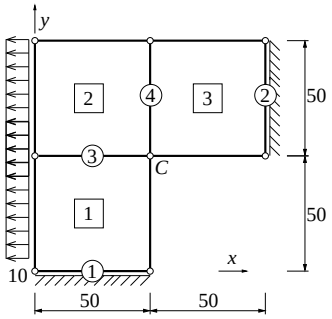

Figure 9: Square plate with a square hole under uniaxial traction.

Local singular solutions at wedge point C are avoided during the *p*-adaptive procedure.

The convergence of the solution is measured using the finite element strain energy U, the energy error norm $|U/U_0|$, and the relative error norm ε_U against the exact energy $U_0 = 0.1556(6)$ given in [8].

The algorithm starts with 24 degrees of freedom, with $d_u^0 = 1$ for the displacement approximation in all elements and $d_t = 0$ on all sides for traction approximations.

The convergence pattern obtained for $\Delta U/U$ against the number of degrees of freedom is presented in Figure 10. The relative energy error admissible is $\varepsilon < 0.001\%$ for the fast and complete algorithms.

As each dof is added sequentially (the best strategy in terms of illustration), the fast *p*-adaptive algorithm converges after 61 steps, while the complete algorithm converges after 43 steps. The convergence pattern obtained for the relative strain energy norm against the number of degrees of freedom is presented in Figure 11.

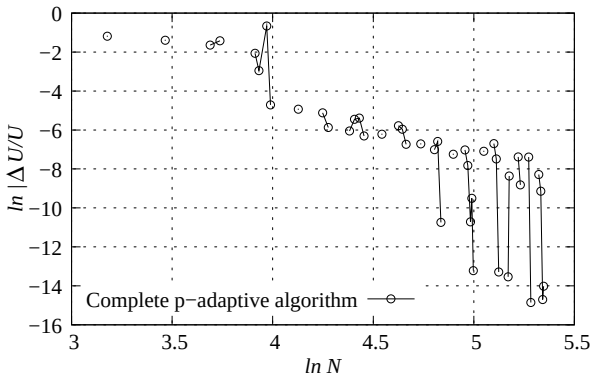

Figure 10: Convergence of the variation of the relative strain energy (plate with a square hole).

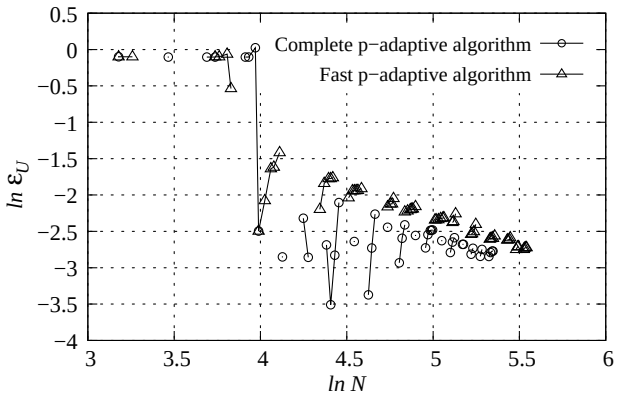

Figure 11: Convergence of the relative error norm in the strain energy, complete algorithm (plate with a square hole).

The final approximation degrees and strain energy for both the complete and fast algorithms are presented in Table 3.

Table 3: Approximation degrees in the domain and boundary and strain energy for the complete (C) and fast (F) *p*-adaptive algorithms (plate with a square hole).

		Domain (d_u)			Boundary (d_t)			
Step	U	1	2	3	1	2	3	4
1	0.02812	1	1	1	0	0	0	0
61(F)	0.15499	15	15	13	12	11	12	12
43(C)	0.15505	13	13	13	4	2	9	9

The final system yields 255 and 210 degrees of freedom for the fast and complete algorithms, respectively. Afterwards, a local singular solution is applied at point C to recover the high gradients locally present. The stress and displacement fields are represented in Figure 12.

The final energy obtained with singular local function at point C is $U = 0.15522$ and $U = 0.15503$ for the complete and fast versions of the algorithm.

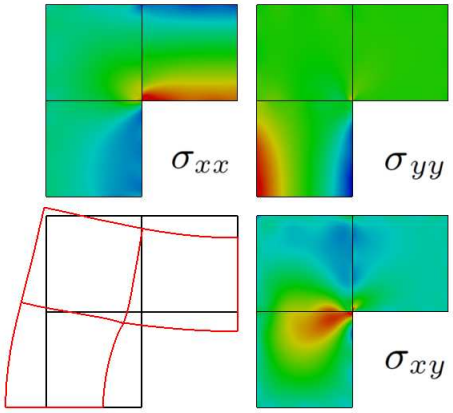

Figure 12: Stress and displacement fields ($4000u$) solution for the complete algorithm. $\sigma_{xx}[-1:5]$; $\sigma_{yy}[-4:3.5]$; $\sigma_{xy}[-0.6:1.5]$ (plate with a square hole).

6.4. Short cantilever plate

The 16 elements cantilever is used to test the robustness of the algorithms and the ability to handle problems with a large number of domain and boundary elements.

The geometry of the model and the adopted mesh is shown in Figure 13. The problem is solved with $E = 2.6$, $\nu = 0.3$ and $p = 1$.

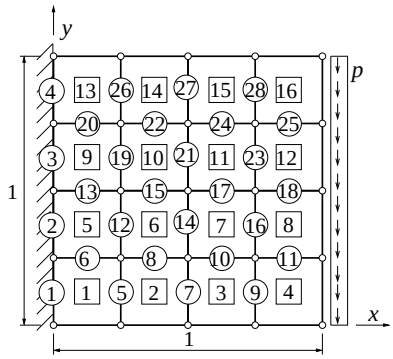

Figure 13: FEM mesh of square plate with 16 elements.

The starting system dimension is 152 d.o.f. The complete algorithm stops after 126 steps with 672 d.o.f and a final energy of $U = 0.378635$, while the fast algorithm needed 157 steps to converge with 776 d.o.f and a final energy of $U = 0.378074$.

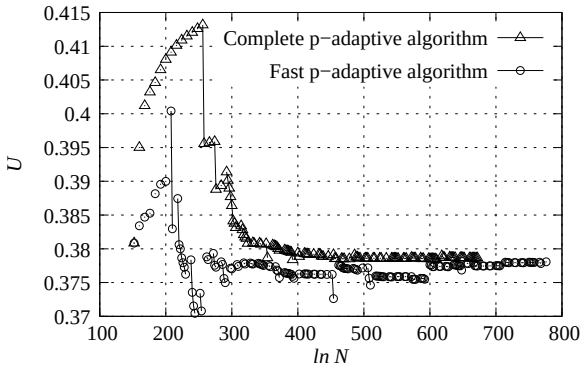

Figure 14: Convergence of strain energy (plate with 16 elements).

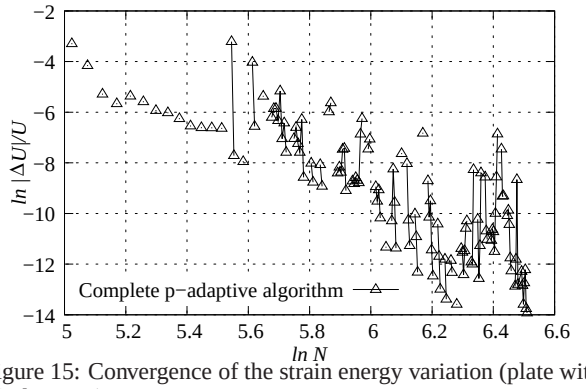

Figure 15: Convergence of the strain energy variation (plate with 16 elements).

The convergence pattern for the strain energy and for the strain energy variation, $|\Delta U|/U$, is presented in Figures 14 and 15.

The final degrees in the domain and on the boundary for the complete and fast algorithms are presented in Figure 16. As expected, higher degrees are obtained for regions of the plate with high stress gradients.

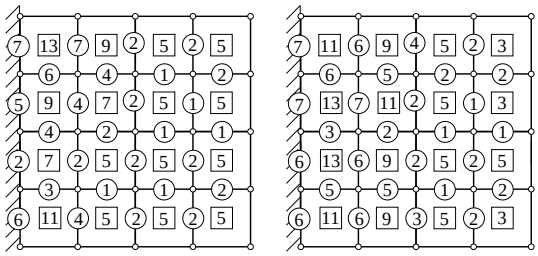

Figure 16: Degrees in the domain and boundary with complete (a) and fast (b) *p*-adaptive algorithms (plate with 16 elements).

The stress and displacement fields are shown in Figure 17.

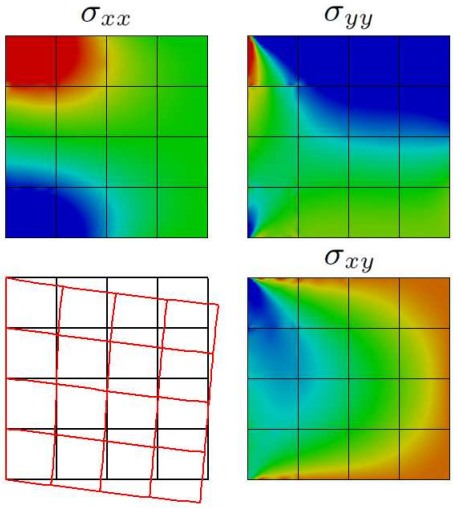

Figure 17: Displacement ($0.001u$) and stress $\sigma_{xx}[-1:1]$; $\sigma_{yy}[-0.7:0.4]$; $\sigma_{xy}[-1.3:0.2]$ fields, complete algorithm (plate with 16 elements).

The results show that the *p*-adaptive algorithm is extremely efficient in identifying the regions necessary for the refinement.

7. Conclusions

The selective *p*-adaptive algorithm included in the preprocessing phase of a special purpose FEM code is an essential tool for selecting the order of approximation basis for a given finite element mesh to solve a given problem. The procedure has proven to be stable and efficient in identifying the regions where refinement is necessary and can be implemented with a minimal computational cost.

The results show that the complete algorithm can select more accurately the order of the approximation functions than the fast version. The large number of steps reported for the different test examples can be misleading as they result from launching the process from the weakest possible starting basis and, also, from the option of enriching individually each basis in each step. The number of steps can be substantially reduced by implementing the strategy of enriching a set of boundary elements at each step.

The use of local singular solutions to enrich the domain bases speeds up convergence and results in a reduction of the polynomial bases implemented in the elements closer to the singularity. However, the overall computational efficiency is affected by the implementation of the semi-analytical procedures required to process the corresponding singular functions present in the (boundary integral) definitions of the structural operators.

Acknowledgements Financial support from research project "Development of Hybrid-Trefftz Finite Element Modelling", PTDC/ECM/70781/2006, funded by Fundação para a Ciência e a Tecnologia and FEDER through Programa POCI 2010, is gratefully acknowledged. The second author acknowledges the "Plurianual" financial support of UNIC by Fundação para a Ciência e a Tecnologia (FCT/MCTES).

References

[1] Cismaşiu, C. The Hybrid-Trefftz Parallel Algorithms for Non-Conventional Finite Element Computations on Distributed Architectures. *Ph.D* Thesis, Universidade Técnica de Lisbon, Instituto Superior Técnico, Lisbon, 2002.

[2] Cismaşiu, I. The Hybrid-Trefftz Displacement Element for Static and Dynamic Structural Analysis Problems. *Ph.D* Thesis, Universidade Técnica de Lisboa, Instituto Superior Técnico, Lisbon, 2000.

[3] Freitas, J.A.T., Almeida, J.P.B.M. and Pereira,E.M.B.R., Non-conventional formulations for the finite element method., *Comput. Mech.* 5/6(23) pp. 488-501, 1999.

[4] Freitas, J. A. T. and Cismaşiu, C., Numerical implementation of hybrid-Trefftz displacement elements., *Comp. Struct.* 73(1-5), pp. 207-225, 1999.

[5] Freitas, J. A. T. and Cismaşiu, C., Adaptive *p*-refinement of hybrid-Trefftz finite element solutions., *Finite Elem. Anal. Des.* 39, pp. 1095-1121, 2003.

[6] Hellan, K., *Introduction to Fracture Mechanics*. McGraw-Hill Book Co., Singapore, 1985.

[7] Robinson, J., *Integrated Theory of Finite Element Methods*. John Wiley and Sons, London, 1973.

[8] Shephard, M. S., Niu, O. and Baehmann, P. L., Some results using stress projectors for error indication and estimation., *Adaptive methods for partial diferential equations*, J. E. Flaherty, P. J. Paslow, M. S. Shephard and J. D. Vasilakis (eds.), SIAM, pp. 83-99, 1989.